

# X-ray Circular Dichroism measured by cross-polarization X-ray Transient Grating

Jérémy R. Rouxel<sup>1</sup>, Riccardo Mincigrucci<sup>2</sup>, Danny Fainozzi<sup>2</sup>, and Claudio Masciovecchio<sup>2</sup>

<sup>1</sup>Chemical Sciences and Engineering Division, Argonne National Laboratory, Lemont, Illinois 60439, United States

<sup>2</sup>Elettra-Sincrotrone Trieste, SS 14 - km 163.5, 34149 Basovizza, Trieste, Italy

December 27, 2023

## Abstract

Measuring natural circular dichroism in the X-ray regime to extract stereochemical information from chiral molecules in solution remains a challenge. This is primarily due to technical limitations of the existing synchrotron sources. It hinders access to measurements of local chirality by exploiting core hole electronic transitions. In response to this challenge, we propose an alternative approach: utilizing XFEL-based cross-polarization X-ray Transient Grating (XTG). This method provides an indirect means to measure X-ray Circular Dichroism (XCD). Notably, our findings reveal that the signal only emerges once the excited cores have undergone dephasing through relaxation. XTG is now routinely measured in the XUV regime, and has recently been made available for hard X-rays. Free electron lasers now offer polarization controls and XTG can be extended to various polarization states for the two pump beams, making XCD measured by XTG feasible at the current state of the art.

## 1 Introduction

The exploration of chiral molecules has been captivating since the pioneering studies conducted by Pasteur in 1848[1]. Since these initial investigations, chirality has held a central role in the field of material sciences and chemistry. Optical Circular Dichroism (CD) spectroscopy stands out as the predominant method for the detection and study of enantiomers[2], i.e. molecules with opposite chirality. This technique relies on the measurement of the difference in absorption exhibited by left and right circularly polarized light. Enantiomers manifest distinct responses to these two forms of light, absorbing them differently. While optical CD is a powerful tool for studying the global chirality of molecules, it encounters limitations in accessing local chirality[3]. Indeed, optical CD primarily relies on transitions involving outer-shell electrons, providing information about the overall molecular structure and chiral properties.

In contrast, X-ray CD, exploiting core hole electronic transitions, offer a more in-depth understanding of the electronic and structural aspects of chiral molecules[4]. This capability enables the examination of local chirality, providing insights into the specific arrangement of the electron density around the chiral centers. Mirror symmetry breaking can occur at specific sites within molecules, at stereogenic centers, or be delocalized everywhere like in helical compounds[5]. Optical CD cannot discriminate these types of chiralities and their localization within molecules. Alternatively, a chiral molecule can provide a vanishing X-ray CD if the probed atom is located far enough from chiral features and is insensitive to them. Despite the significance of natural X-ray Circular Dichroism (XCD), successful experiments have been relatively few, typically limited to crystals or the gas phase[6, 7, 8]. The primary challenge lies in the subtle difference in signal arising from the differential absorption of left- and right-polarized photons. As a consequence, the experimental detection of natural XCD, especially in more complex environments like solutions, has proven to be a formidable task.

Addressing this challenge requires innovative approaches and advancements in experimental techniques to enhance the signal-to-noise ratio and improve the sensitivity of XCD measurements. Overcoming these limitations is crucial for unlocking the full potential of XCD in providing detailed insights into the structural and electronic features of chiral molecules, which is essential for various scientific disciplines, including chemistry, biochemistry, and materials science[9, 10, 11, 12]. In the present work

we theoretically demonstrate that cross-polarization X-ray Transient Grating (XTG) provides an indirect method for measuring X-ray CD.

XTG is a four-wave-mixing(4WM) technique in which two coincidence pump beams with the same spectral profile are crossed with an angle  $2\theta$  on a sample and create a transient interference pattern of excitation[13]. The diffraction of a delayed probe emitted in a background free direction[14] is then detected. Similar to standard pump-probe experiments, the diffracted intensity contains information about ultrafast relaxation pathways. Additionally, the transient grating signal can also decay by transport of the excited carriers, which is then monitored by the XTG techniques[15]. TG has been commonly employed since the 80s in optical laboratories, and the work of Bencivenga et al.[16, 17, 18] at the FEL FERMI has made TG experiments possible in the XUV using the beam crossing geometry in the last decade. Recently, the use of diffractive optics has opened it in the hard X-ray regime[19].

As a 4WM technique, XTG can be described by third-order nonlinear polarizability  $P_{\text{XTG}}^{(3)}$ , itself containing a convolution between the four-point matter correlation functions and the incoming field time envelopes. However, if the delay  $\tau$  between the two pumps and the probe is longer than the matter electronic decoherence time, the matter correlation function can be factorized into two two-point correlation functions. This is typically the case when thermal transport is investigated and the transport during the delay  $\tau$  is essentially classical. In this case, the transient excitation grating is used to deposit energy, in the form of heat after relaxation, and quantum features are lost. While it may be detrimental to measure, e.g. core-hole relaxation using XTG, this can be used as an indirect measure of linear responses, including the chiral linear response.

In the optical regime, the idea originates from foundational works of Fayer[20, 21] and Terazima[22, 23]. Using crossed polarization states, they showed that the polarization grating can be converted into an intensity grating if the excited matter possesses chirality, i.e. a differential absorption of left and right circular polarization of light (CPL). In the following, we show how this allows the measure of X-ray Circular Dichroism (XCD) indirectly. In the optical regime, the widespread availability of commercially available spectrometer for CD has hindered the development of this more complicated, indirect measurement. Additionally, homodyne-detected signals are not sensitive to sign changes in the signal amplitudes. As a consequence, XTG-detected XCD cannot distinguish opposite enantiomers. It is still sensitive to chirality in the sense that the signal vanishes in achiral systems, but is not enantioselective. However, in the X-rays or EUV, XCD is more challenging due to the difficulty to obtain left and right CPL with high stability and polarization purity. For example, FERMI already offers[24, 25] the required cross-polarization schemes, making XTG-measured XCD readily available.

In this work, we first review general signal expressions of the XTG signal. Second, we discuss the geometry of the cross-polarization XTG. Third, we show how the rotatory strength emerges from dephased XTG signal. Finally, a simulation of XTG-measured XCD from L-tryptophan is made as an illustration.

## 2 Signal definition

The XTG signal is a spontaneous, coherent signal and can thus be expressed as the amplitude squared of the nonlinear matter polarization[26]:

$$S(\tau) = \int dt |P_{\text{XTG}}^{(3)}(t, \tau)|^2 \quad (1)$$

where  $P_{\text{XTG}}^{(3)}$  is the third-order matter polarization emitting a spontaneous field in the  $k_s = k_1 - k_2 + k_3$  phase-matching direction, see Fig.1.  $\tau$  is the delay between the EUV pumps and the probe pulse and  $t$  is the integration time of the detector. The nonlinear polarization  $P_{\text{XTG}}^{(3)}$  is generated by perturbative interactions with two coincident, non-collinear pump pulses  $E_1$  and  $E_2$  and a delayed diffracted probe  $E_3$ . As shown in Fig. 1, pulses  $E_1$  and  $E_2$  are cross-polarized (red marks in the scheme). The probe polarization is unimportant for the proposed homodyne-detected XTG and is thus left unspecified. At FELs,  $E_1$  and  $E_2$  are high energy pulses (EUV or X-ray), while  $E_3$  is either optical or high frequency depending on the periodicity of the generated transient grating. Full X-ray (pumps and probe) XTG is still a challenging technique to implement[19].

Our derivation for XTG-detected XCD signal is based on the multipolar field-matter interaction Hamiltonian truncated at the magnetic dipole order[27]:

$$H_{\text{int}}(t) = -\boldsymbol{\mu} \cdot \mathbf{E}(t) - \mathbf{m} \cdot \mathbf{B}(t) \quad (2)$$

where  $\boldsymbol{\mu}$  and  $\mathbf{m}$  are the electric and magnetic transition dipoles respectively and  $\mathbf{E}$  and  $\mathbf{B}$  are the incoming electric and magnetic field amplitudes. We do not consider electric quadrupole coupling in the following since it vanishes upon rotational averaging over random sample orientation[27].

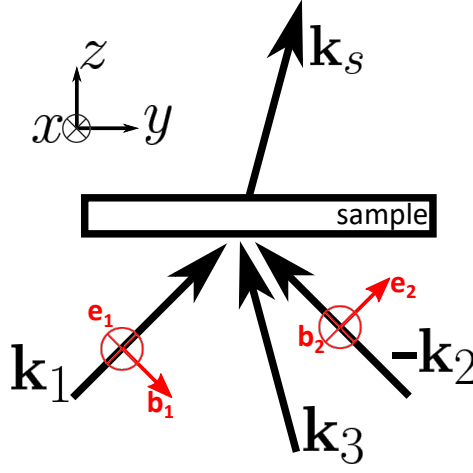


Figure 1: Geometry of cross-polarization XTG setup. The polarizations  $e_1$  and  $e_2$  of pulses  $E_1$  and  $E_2$  are orthogonal to each other. The corresponding polarizations  $b_1$  and  $b_2$  of the magnetic fields  $B_1$  and  $B_2$  are also shown. The TG signal is emitted in the phase-matching direction  $k_s = k_1 - k_2 + k_3$ .

The polarization  $P_{\text{XTG}}^{(3)}$  is given by a summation over the ladder diagrams relevant for the XTG technique[26] and shown in Fig. 2:

$$P_{\text{XTG}}^{(3)}(t, \tau) = \sum_i P_{D_i}(t, \tau) \quad (3)$$

with

$$P_{D_1}(t, \tau) = \left(-\frac{i}{\hbar}\right)^3 \int dt_3 dt_2 dt_1 \langle \mu_L \mathcal{G}(t_3) \mu_R \mathcal{G}(t_2) \mu_R \mathcal{G}(t_1) \mu_L \rangle E_3(t-t_3) E_2^*(t-t_3-t_2+\tau) E_1(t-t_3-t_2-t_1+\tau) \quad (4)$$

$$P_{D_2}(t, \tau) = \left(-\frac{i}{\hbar}\right)^3 \int dt_3 dt_2 dt_1 \langle \mu_L \mathcal{G}(t_3) \mu_R \mathcal{G}(t_2) \mu_L \mathcal{G}(t_1) \mu_R \rangle E_3(t-t_3) E_1(t-t_3-t_2+\tau) E_2^*(t-t_3-t_2-t_1+\tau) \quad (5)$$

$$P_{D_3}(t, \tau) = \left(-\frac{i}{\hbar}\right)^3 \int dt_3 dt_2 dt_1 \langle \mu_L \mathcal{G}(t_3) \mu_L \mathcal{G}(t_2) \mu_L \mathcal{G}(t_1) \mu_L \rangle E_3(t-t_3) E_2^*(t-t_3-t_2+\tau) E_1(t-t_3-t_2-t_1+\tau) \quad (6)$$

$$P_{D_4}(t, \tau) = \left(-\frac{i}{\hbar}\right)^3 \int dt_3 dt_2 dt_1 \langle \mu_L \mathcal{G}(t_3) \mu_L \mathcal{G}(t_2) \mu_R \mathcal{G}(t_1) \mu_R \rangle E_3(t-t_3) E_1(t-t_3-t_2+\tau) E_2^*(t-t_3-t_2-t_1+\tau) \quad (7)$$

where  $\mu_L$  and  $\mu_R$  correspond to interaction on the left or the right of the matter density matrix, leading to different phases for different interaction pathways. Eqs.4 to 7 can be read out directly from the diagrams in a systematic manner[26]. As a general 4WM technique, the nonlinear polarization is thus given by the convolution of a four-point matter correlation function with the temporal envelopes of the incoming pulses.

In the cross-polarization XTG setup, magnetic dipole interactions with the EUV beams are considered. Each of the 4 diagrams in Fig. 2 can be separated into 3 contributions corresponding to different multipolar interaction pathways. For example, the contributions from diagram  $D_1$  in Fig. 2 to the signal is now:

$$P_{D_1}^{\mu\mu}(t, \tau) = \left(-\frac{i}{\hbar}\right)^3 \int dt_3 dt_2 dt_1 \langle \mu_L \mathcal{G}(t_3) \mu_R \mathcal{G}(t_2) \mu_R \mathcal{G}(t_1) \mu_L \rangle E_3(t-t_3) E_2^*(t-t_3-t_2+\tau) E_1(t-t_3-t_2-t_1+\tau) \quad (8)$$

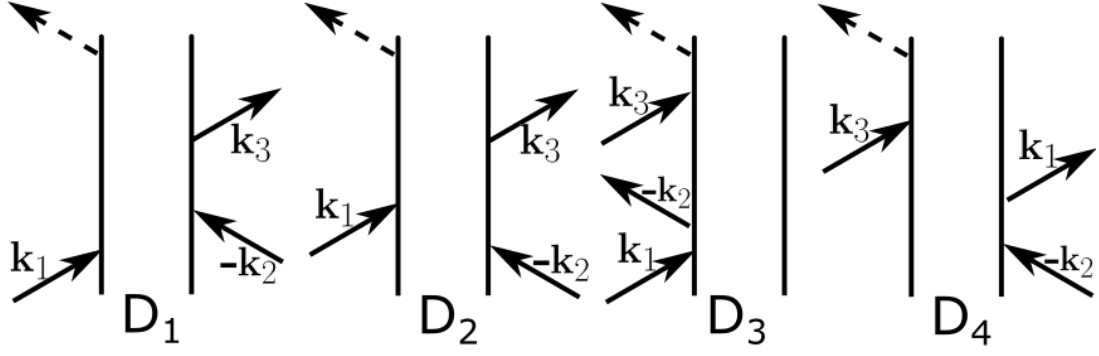


Figure 2: Ladder diagrams contributing to the XTG signal. Interactions with  $k_1$  and  $k_2$  can be either with electric dipole or magnetic dipole coupling.

$$P_{D_1}^{\mu m}(t, \tau) = \left(-\frac{i}{\hbar}\right)^3 \int dt_3 dt_2 dt_1 \langle \mu_L \mathcal{G}(t_3) \mu_R \mathcal{G}(t_2) \mu_R \mathcal{G}(t_1) m_L \rangle E_3(t-t_3) E_2^*(t-t_3-t_2+\tau) B_1(t-t_3-t_2-t_1+\tau) \quad (9)$$

$$P_{D_1}^{m\mu}(t, \tau) = \left(-\frac{i}{\hbar}\right)^3 \int dt_3 dt_2 dt_1 \langle \mu_L \mathcal{G}(t_3) \mu_R \mathcal{G}(t_2) m_R \mathcal{G}(t_1) \mu_L \rangle E_3(t-t_3) B_2^*(t-t_3-t_2+\tau) E_1(t-t_3-t_2-t_1+\tau) \quad (10)$$

where  $P_{D_1}^{m\mu}(t, \tau)$  is an electric-dipole only contribution, not sensitive to chirality, and that vanishes when using a cross polarization scheme.  $P_{D_1}^{\mu m}(t, \tau)$  and  $P_{D_1}^{m\mu}(t, \tau)$  have one magnetic dipole interaction with either the pulse  $E_1$  or  $E_2$  respectively.

Diagrams in Fig. 2 assumes that the pumps and the probe are well separated temporally, so partial time-ordering of the interactions can be ensured. Near time zero, when the pumps and the probe temporally overlap, additional diagrams must be taken into account, shown in Fig. 3. For example, self-diffraction is a degenerate XTG signal with no delayed probe and in which the "probe" interaction is achieved with one of the pump pulses. This experimentally simpler technique (no delay  $\tau$  to implement) would require the addition of these two contributions in the signal description.

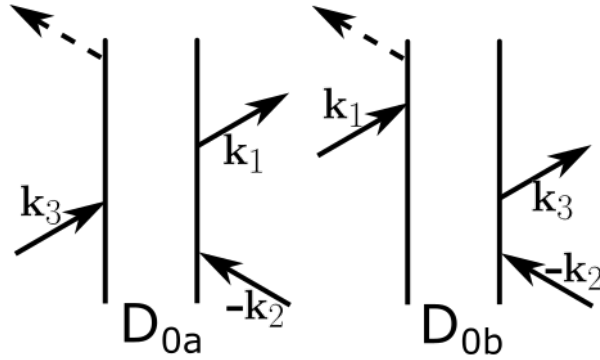


Figure 3: Additional ladder diagrams contributing to the XTG signal when the delay between the EUV pumps and the probe is small.

### 3 Geometry for cross-polarized XTG

Some geometric identities are needed to describe the signal. We use the frame of coordinates shown in Fig. 1. The pulse  $E_1$  and  $E_2$  are linearly polarized along the  $x$  and  $y$  axes respectively, and have an angle  $\pm\theta$  with respect to the  $z$  axis. Using simple algebra, we can show that the polarizations and wavevectors are:

$$\begin{aligned} e_1 &= e_x \\ e_2 &= \cos\theta e_y + \sin\theta e_z \\ k_1 \cdot r &= k_X(y \sin\theta + z \cos\theta) \\ k_2 \cdot r &= k_X(-y \sin\theta + z \cos\theta) \end{aligned} \quad (11)$$

It will be convenient in the following to use the circular polarization basis defined as:

$$\mathbf{e}_L = \frac{1}{\sqrt{2}} \begin{pmatrix} 1 \\ i \\ 0 \end{pmatrix} \quad \mathbf{e}_R = \frac{1}{\sqrt{2}} \begin{pmatrix} 1 \\ -i \\ 0 \end{pmatrix} \quad (12)$$

We also define a polarization basis for the  $\mathbf{B}$  field as:

$$\mathbf{b}_L = \mathbf{e}_z \times \mathbf{e}_L = -i\mathbf{e}_L \quad (13)$$

$$\mathbf{b}_R = \mathbf{e}_z \times \mathbf{e}_R = i\mathbf{e}_R \quad (14)$$

Using the spherical basis, the fields can be written as:

$$\mathbf{E}_1 = E_x(t) \frac{1}{\sqrt{2}} (\mathbf{e}_L + \mathbf{e}_R) e^{ik_X(y \sin \theta + z \cos \theta)} \quad (15)$$

$$\mathbf{E}_2 = E_x(t) \left( -i \frac{\cos \theta}{\sqrt{2}} (\mathbf{e}_L - \mathbf{e}_R) + \mathbf{e}_z \sin \theta \right) e^{ik_X(-y \sin \theta + z \cos \theta)} \quad (16)$$

$$\mathbf{B}_1 = \frac{E_x(t)}{c} \left( \frac{\cos \theta}{\sqrt{2}} (\mathbf{b}_L + \mathbf{b}_R) - \sin \theta \mathbf{e}_z \right) e^{ik_X(y \sin \theta + z \cos \theta)} \quad (17)$$

$$\mathbf{B}_2 = \frac{E_x(t)}{c} \frac{1}{\sqrt{2}} (-i) (\mathbf{b}_L - \mathbf{b}_R) e^{ik_X(-y \sin \theta + z \cos \theta)} \quad (18)$$

Finally, we provide some identities involving scalar products used in the following:

$$\begin{aligned} \mathbf{e}_L \cdot \mathbf{e}_L^* &= \mathbf{e}_R \cdot \mathbf{e}_R^* = 1 \\ \mathbf{e}_L \cdot \mathbf{e}_R^* &= \mathbf{e}_R \cdot \mathbf{e}_L^* = 0 \\ \mathbf{e}_L \cdot \mathbf{b}_L^* &= \mathbf{e}_R^* \cdot \mathbf{b}_R = i \\ \mathbf{e}_R \cdot \mathbf{b}_R^* &= \mathbf{e}_L^* \cdot \mathbf{b}_L = -i \end{aligned} \quad (19)$$

## 4 XCD measured by dephased cross-polarization XTG

We now show how the chiral-sensitivity appears in cross-polarization XTG. To simplify the discussion, we consider the impulsive limit for the 3 incoming pulses:  $E_i(t) = E_i \delta(t)$ . The impulsive limit cannot include a complete description of resonant spectral features, which are discussed in Appendix A, but is convenient to show how the polarization algebra eliminates the achiral contribution to the XTG signal. We also restrict the discussion to diagram  $D_1$ , since the other three give similar contributions. In the impulsive limit,  $P_{D_1}(t, \tau)$  becomes:

$$P_{D_1}^{\mu\mu}(t, \tau) = \left(-\frac{i}{\hbar}\right)^3 \langle \boldsymbol{\mu}_L \mathcal{G}(t) \boldsymbol{\mu}_R \mathcal{G}(\tau) \boldsymbol{\mu}_R \mathcal{G}(0) \boldsymbol{\mu}_L \rangle E_3 E_2^* E_1 \quad (20)$$

Rigorously, the XTG response involves a four-point correlation function. However, the core excitation triggered by the EUV pulses are usually short lived (tens of fs, or less) and the signal dephases completely during the pump-probe delay  $\tau$ . This implies that the correlation function can be factorized into two two-point correlation functions[28] and that  $\mathcal{G}(\tau)$  is replaced by a classical propagator  $U(\tau)$ . If the excited carriers can move during that time,  $U(\tau)$  describes the classical transport that is measured in long delay TG experiments.

The contribution  $P_{D_1}(t, \tau)$  becomes:

$$P_{D_1}^{\mu\mu}(t, \tau) = \left(-\frac{i}{\hbar}\right)^3 \langle \boldsymbol{\mu}_L \mathcal{G}(t) \boldsymbol{\mu}_R \rangle U(\tau) \langle \boldsymbol{\mu}_R \boldsymbol{\mu}_L \rangle E_3 E_2^* E_1 \quad (21)$$

If the sample is constituted of randomly oriented components (for example molecules in liquid phase or isotropic powder form), the correlation functions must be averaged over orientations. This leads to:

$$P_{D_1}^{\mu\mu}(t, \tau) = \left(-\frac{i}{\hbar}\right)^3 \frac{1}{9} \langle \boldsymbol{\mu}_L \cdot \boldsymbol{\mu}_R \rangle U(\tau) \langle \boldsymbol{\mu}_R \cdot \boldsymbol{\mu}_L \rangle E_3 E_2^* \cdot E_1 \quad (22)$$

Similarly, for the magnetic components, we obtain:

$$P_{D_1}^{\mu m}(t, \tau) = \left(-\frac{i}{\hbar}\right)^3 \frac{1}{9} \langle \boldsymbol{\mu}_L \cdot \boldsymbol{\mu}_R \rangle U(\tau) \langle \boldsymbol{\mu}_R \cdot \mathbf{m}_L \rangle E_3 E_2^* \cdot \mathbf{B}_1 \quad (23)$$

$$P_{D_1}^{m\mu}(t, \tau) = \left(-\frac{i}{\hbar}\right)^3 \frac{1}{9} \langle \boldsymbol{\mu}_L \cdot \boldsymbol{\mu}_R \rangle U(\tau) \langle \mathbf{m}_R \cdot \boldsymbol{\mu}_L \rangle E_3 \mathbf{B}_2^* \cdot E_1 \quad (24)$$

Using the identities of the previous section, we can finally calculate the various dot products as follow:

$$\mathbf{E}_1 \cdot \mathbf{E}_2^* = -i \frac{E_X^2}{2} \cos \theta e^{2ik_{xy} \sin \theta} (\mathbf{e}_L + \mathbf{e}_R) \cdot (\mathbf{e}_L - \mathbf{e}_R) = 0 \quad (25)$$

$$\mathbf{E}_1 \cdot \mathbf{B}_2^* = \frac{E_X^2}{c} e^{2ik_{xy} \sin \theta} \quad (26)$$

$$\mathbf{E}_1 \cdot \mathbf{B}_2^* = \frac{E_X^2}{c} \cos^2 \theta e^{2ik_{xy} \sin \theta} \quad (27)$$

The signal contributions from diagrams  $D_1$  is thus:

$$\begin{aligned} P_{D_1}(t, \tau) &= P_{D_1}^{\mu\mu}(t, \tau) + P_{D_1}^{\mu m}(t, \tau) + P_{D_1}^{mm}(t, \tau) \\ &= 0 + \frac{1}{9c} \frac{i}{\hbar^3} \langle \boldsymbol{\mu}_L \cdot \boldsymbol{\mu}_R \rangle U(\tau) \left( \langle \boldsymbol{\mu}_R \cdot \mathbf{m}_L \rangle + \cos^2 \theta \langle \mathbf{m}_R \cdot \boldsymbol{\mu}_L \rangle \right) E_3 E_X^2 \cos \theta \\ &= \frac{1 + \cos^2 \theta}{9c} \frac{i}{\hbar^3} \langle \boldsymbol{\mu}_L \cdot \boldsymbol{\mu}_R \rangle U(\tau) \langle \boldsymbol{\mu}_R \cdot \mathbf{m}_L \rangle E_3 I_X \end{aligned} \quad (28)$$

where  $I_X = E_X^2$  is the intensity of the X-ray pulses. In Eq. 28, we have used that  $\langle \boldsymbol{\mu}_R \cdot \mathbf{m}_L \rangle = \langle \mathbf{m}_R \cdot \boldsymbol{\mu}_L \rangle$  for linear absorption terms.

Hence, the pseudo-scalar  $\boldsymbol{\mu} \cdot \mathbf{m}$  appears in the leading term to the cross-polarized XTG signal. It is closely related to the rotatory strength given by  $R_{cg} = \text{Im}(\boldsymbol{\mu}_{gc} \cdot \mathbf{m}_{cg})$  where  $g$  and  $c$  are the electronic ground and core-excited states respectively. The rotatory strength  $R_{cg}$  is closely related to the differential absorption between left and right CPL measured in standard CD measurement[29] by:

$$R_{cg} \approx \frac{3 \ln 10}{16\pi^2 c N_a} \int_{\omega_{cg}-\epsilon}^{\omega_{cg}+\epsilon} d\omega \frac{\epsilon_L(\omega) - \epsilon_R(\omega)}{\omega} \quad (29)$$

where  $\epsilon_L$  and  $\epsilon_R$  are the molar extinction coefficients measured with left and right CPL respectively. The measured XCD signal is given by  $S_{CD}(\omega) = A_L(\omega) - A_R(\omega)$  where  $A(\omega) = \epsilon(\omega)cl$  is the absorbance,  $c$  the sample concentration and  $l$  the interaction length.

Diagrams  $D_1$  to  $D_4$  give the same contribution within the approximations discussed above, and the nonlinear polarization  $P_{\text{XTG}}^{(3)}$ , Eq. 3, is 4 times the result given in Eq. 28.

When the spectral bandwidth of the incoming pump is accounted for, see Appendix A, the cross polarization XTG signal is given by:

$$S_{\text{XTG}}(\tau, \omega_p) = \left| 4 \frac{1 + \cos^2 \theta}{9\hbar^3 c} \langle \boldsymbol{\mu}_L \mathcal{G}(\omega_{pr}) \boldsymbol{\mu}_R \rangle U(\tau) \langle \boldsymbol{\mu}_R \mathcal{G}(\omega_p) \mathbf{m}_L \rangle E_3 I_X \right|^2 \quad (30)$$

$$\propto |S_{CD}(\omega_p)|^2 \quad (31)$$

where  $\omega_p$  is the pump central frequencies and  $\omega_{pr}$  is the probe central frequency. The delay  $\tau$  change the prefactor of the signal through the classical propagator  $U(\tau)$  and is independent from the chiral observable. By scanning  $\omega_p$  at a fixed delay  $\tau$ , one can reconstruct the amplitude squared of the XCD signal. By changing  $\omega_p$ , the phase matching condition is modified and one must use a detector able to follow the corresponding angular change, use a sufficiently large array detector or account for the losses due to partial phase matching. We stress the fact that while cross-polarization XTG is sensitive to chirality, i.e. it vanishes in achiral samples, it is unable to discriminate opposite enantiomers since the rotatory strength is squared. Heterodyne-detected XTG could be the key to discriminate enantiomers by measuring the signal phase.

If the polarization of the two pumps is not perfectly crossed or if their intensity is not equal, achiral contributions would appear as potential spurious signal. For example, if we consider a more general elliptical polarization for  $\mathbf{E}_1$ :

$$\mathbf{E}_1 = E_{1x} \mathbf{e}_x + E_{1y} e^{i\varphi} \mathbf{e}_y = \frac{1}{\sqrt{2}} (E_{1x} - iE_{1y} e^{i\varphi}) \mathbf{e}_L + \frac{1}{\sqrt{2}} (E_{1x} + iE_{1y} e^{i\varphi}) \mathbf{e}_R \quad (32)$$

then the dot product for the achiral contribution would not vanish anymore:

$$\begin{aligned} \mathbf{E}_1 \cdot \mathbf{E}_2^* &= \frac{E_2}{2} (-i) \cos \theta e^{2ik_{xy} \sin \theta} \left( E_{1x} (\mathbf{e}_L + \mathbf{e}_R) \cdot (\mathbf{e}_L - \mathbf{e}_R) + E_{1y} e^{i\varphi} (\mathbf{e}_L - \mathbf{e}_R) \cdot (\mathbf{e}_L - \mathbf{e}_R) \right) \\ &= E_2 E_{1y} e^{i\varphi} \cos \theta e^{2ik_{xy} \sin \theta} \end{aligned} \quad (33)$$

## 5 Application to the chiral response of L-tryptophan

We have calculated the cross-polarized XTG signal for a randomly oriented ensemble of L-tryptophan (Fig. 4a insert) with an X-ray incident pulse tuned at the C K-edge ( $\omega_p=288.5 - 294$  eV). The geometry was optimized at the HF/cc-pVDZ level of theory using the Molpro program package[30].

The core excited states are then calculated in separate RASSCF calculations, by freezing the optimization of the 1s core orbitals of each C atom, rotating them into the active space and restricting their occupation to a single electron. Computations were done at the RASSCF(9,7)/cc-pVDZ level of theory. The active space contained the singly occupied 1s orbital of the chosen C atom and valence orbitals ranging from HOMO-3 to LUMO+1.

In Fig. 4, the XCD and cross-polarized XTG signals are shown in panels a and b respectively. The XCD signal is computed using  $S_{\text{XCD}}(\omega_p) = -\text{Im}\langle \mu_R \mathcal{G}(\omega_1) \mathbf{m}_L \rangle$  where  $\langle \mu_R \mathcal{G}(\omega_1) \mathbf{m}_L \rangle$  is given in Eq.38. The stick spectrum of the transitions is shown in Fig. 4a and a phenomenological lifetime broadening for the C 1s excited of 0.1 eV was applied to display the spectrum[31]. The cross-polarized XTG has been computed using Eq.30. A simple classical propagator of the form:

$$U(\tau) = \frac{1}{2} \left( 1 + \text{erf}\left(\frac{\tau}{t_r}\right) \right) e^{-\tau/t_d} \quad (34)$$

where  $t_r = 0.5$  ps and  $t_d = 5$  ps accounts for the instrument response function and for the classical relaxation time respectively. Typically,  $t_d$  describes a thermal decay, by diffusion or vibrational relaxation. As seen in Fig.4b, horizontal slices of the cross-polarized XTG signal recover the amplitude square of the XCD signal. Systems with short dephasing time and long thermal relaxation would allow for a larger time-window to detect XCD using the XTG signal.

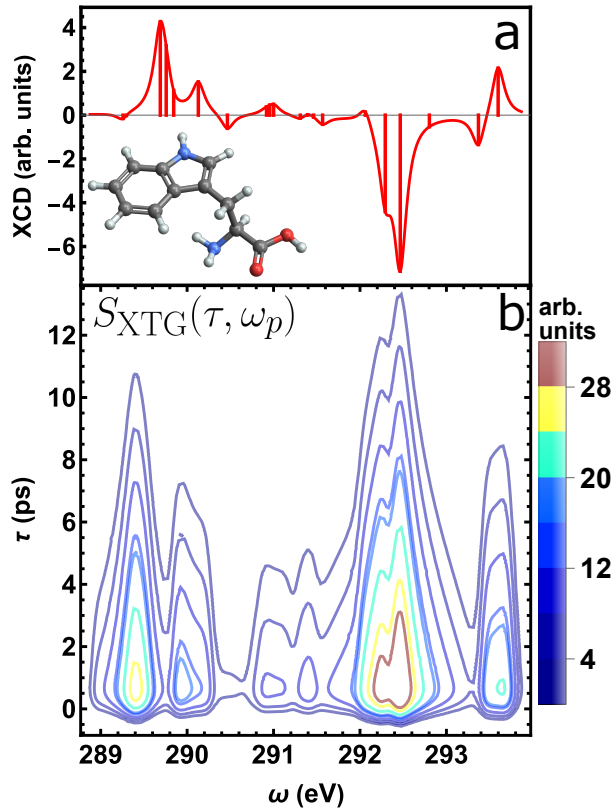


Figure 4: a) XCD signal of L-tryptophan (structure in insert) at the carbon K-edge. b) Cross-polarized XTG signal on the same molecule.

## 6 Conclusion

In this study, we showcase that homodyne-detected cross-polarized X-ray Transient Grating is a remarkably sensitive technique for probing molecular chirality. In the optical case, as discussed by Terazima[22], the dephasing time can exhibit a relatively prolonged duration. This characteristic imposes limitations

on the technique, particularly for longer delay times (hundreds of ps), where the transient grating could already show a significant decay. In scenarios where core-holes are excited, the dephasing time is notably shorter than the core lifetime, typically falling within the range of approximately of few femtoseconds. This introduces the possibility of factorizing the X-ray Transient Grating (XTG) matter correlation function at very short times. In the case of pulses lasting a few tens of femtoseconds, the phenomenon of decoherence can manifest within the pulse duration itself. This implies that factorization is consistently possible, and the signal effectively probes rotatory strengths even in scenarios where no delays are introduced between the pump and the probe pulses. If this hypothesis proves to be accurate, it would open the door to probing chirality using self-diffraction. In the self-diffraction scenario, two pulses intersect on the sample, and one of the two pumps undergoes diffraction by the transient grating that is forming. This corresponds to a degenerate XTG at zero delay (the probe pulse is one of the pump pulses)[32].

If the cross-polarization XTG experiment with attosecond pulses was pursued, it could be expected that the full four-point correlation function would have to be considered fully in that case. Deviation from the XCD measurement could in turn be considered as a signature of the core-hole decoherence process. Finally, if the polarization of the emitted electric field  $E_s$  were to be resolved, it would be possible to consider cross-polarization contributions from  $E_3$  and  $E_s$ , allowing the detection of rotatory strength after the delay  $\tau$ .

## A Spectral measurement by frequency scanning

In this appendix, we show how the spectral features of XCD are accounted for when the central frequency  $\omega_p$  of the pump pulses is scanned. Starting from Eq. 9 for  $P_{D_1}^{\mu m}(t, \tau, \omega_p)$  and Fourier transforming the pulse  $E_1$ , we get

$$P_{D_1}^{\mu m}(t, \tau, \omega_p) = \left(-\frac{i}{\hbar}\right)^3 \int dt_3 dt_2 dt_1 \frac{d\omega_1}{2\pi} \langle \mu_L \mathcal{G}(t_3) \mu_R \mathcal{G}(t_2) \mu_R \mathcal{G}(t_1) \mathbf{m}_L \rangle \times E_3(t-t_3) E_2^*(t-t_3-t_2+\tau) B_1(\omega_1) e^{-i\omega_1(t-t_3-t_2-t_1+\tau)} \quad (35)$$

where  $B_1(\omega) = \int dt B_1(t) e^{i\omega t}$ . The Fourier transform over the propagator  $\mathcal{G}(t_1)$  is given by:

$$\mathcal{G}(\omega_1) = \sum_c \frac{|cg\rangle \langle cg|}{\omega - \omega_{cg} + i\Gamma_{cg}} \quad (36)$$

where the Liouville space double bracket notation[26] has been used.  $c$  and  $g$  represent the core-excited states and the ground state respectively, and  $\Gamma_{cg}$  are phenomenological broadening rates for core-excited states.

When the pump pulses spectral bandwidth is narrow compared to the core excited state lineshape, we can approximate the spectral envelope by a Dirac delta function centered at the pump frequencies  $\omega_p$ :  $B_1(\omega_1) = B_1 \delta(\omega_1 - \omega_p)$ . The temporal envelope of  $E_2$ , which has the same spectral profile as  $E_1$ , is short compared to the classical dynamics following the core hole dephasing time and can still be kept as impulsive in time domain. Finally, the temporal envelope of the probe pulse is independent of that process and is taken as impulsive for simplicity. Under these approximations, Eq. 35 becomes:

$$P_{D_1}^{\mu m}(t, \tau, \omega_p) = \left(-\frac{i}{\hbar}\right)^3 \int dt_2 \frac{d\omega_1}{2\pi} \langle \mu_L \mathcal{G}(t) \mu_R \mathcal{G}(t_2) \mu_R \mathcal{G}(\omega_1) \mathbf{m}_L \rangle E_3 E_2^*(-t_2 + \tau) B_1(\omega_1) e^{i\omega_1(t_2 - \tau)} = \left(-\frac{i}{\hbar}\right)^3 E_3 E_2^* B_1 \langle \mu_L \mathcal{G}(t) \mu_R \rangle U(\tau) \langle \mu_R \mathcal{G}(\omega_1) \mathbf{m}_L \rangle \quad (37)$$

where

$$\langle \mu_R \mathcal{G}(\omega_p) \mathbf{m}_L \rangle = \sum_c \frac{\boldsymbol{\mu}_{gc} \cdot \mathbf{m}_{cg}}{\omega_p - \omega_{cg} + i\Gamma_{cg}} \quad (38)$$

## Acknowledgements

Work by JRR was supported by the U.S. Department of Energy (DOE), Office of Science, Basic Energy Science (BES), Chemical Sciences, Geosciences and Biosciences Division (CSGB) under Contract No. DE-AC02-06CH11357.

## References

- [1] Louis Pasteur. Sur les relations qui peuvent exister entre la forme cristalline, la composition chimique et le sens de la polarization rotatoire. *Annales Chimie Phys.*, 24:442–459, 1848.
- [2] Nina Berova, Koji Nakanishi, and Robert W Woody. *Circular dichroism: principles and applications*. John Wiley & Sons, 2000.
- [3] Jérémy R Rouxel and Shaul Mukamel. Molecular chirality and its monitoring by ultrafast x-ray pulses. *Chemical Reviews*, 122(22):16802–16838, 2022.
- [4] Jérémy R Rouxel, Vladimir Y Chernyak, and Shaul Mukamel. Non-local real-space analysis of chiral optical signals. *Chemical science*, 7(11):6824–6831, 2016.
- [5] Victor M Freixas, Jérémy R Rouxel, Yeonsig Nam, Sergei Tretiak, Niranjan Govind, and Shaul Mukamel. X-ray and optical circular dichroism as local and global ultrafast chiral probes of [12] helicene racemization. *Journal of the American Chemical Society*, 145(38):21012–21019, 2023.
- [6] Lucilla Alagna, Tommaso Proserpi, Stefano Turchini, José Goulon, Andrei Rogalev, Chantal Goulon-Ginet, Calogero R Natoli, Robert D Peacock, and Brian Stewart. X-ray natural circular dichroism. *Physical review letters*, 80(21):4799, 1998.
- [7] José Goulon, Chantal Goulon-Ginet, Andrei Rogalev, Vincent Gotte, Cécile Malgrange, Christian Brouder, and Calogero R Natoli. X-ray natural circular dichroism in a uniaxial gyrotropic single crystal of liio 3. *The Journal of chemical physics*, 108(15):6394–6403, 1998.
- [8] Mikhail S Platunov, Irina A Gudim, Elena N Ovchinnikova, Ksenia A Kozlovskaya, Fabrice Wilhelm, Andrei Rogalev, Amir Hen, Vsevolod Y Ivanov, Alexander A Mukhin, and Vladimir E Dmitrienko. X-ray natural circular dichroism imaging of multiferroic crystals. *Crystals*, 11(5):531, 2021.
- [9] Barbara Kasprzyk-Hordern. Pharmacologically active compounds in the environment and their chirality. *Chemical Society Reviews*, 39(11):4466–4503, 2010.
- [10] Silas W Smith. Chiral toxicology: it’s the same thing... only different. *Toxicological sciences*, 110(1):4–30, 2009.
- [11] Zuoqia Wang, Feng Cheng, Thomas Winsor, and Yongmin Liu. Optical chiral metamaterials: a review of the fundamentals, fabrication methods and applications. *Nanotechnology*, 27(41):412001, 2016.
- [12] David B Cline. On the physical origin of the homochirality of life. *European Review*, 13(S2):49–59, 2005.
- [13] Emily J Brown, Qingguo Zhang, and Marcos Dantus. Femtosecond transient-grating techniques: Population and coherence dynamics involving ground and excited states. *The Journal of chemical physics*, 110(12):5772–5788, 1999.
- [14] John T Fourkas and MD Fayer. The transient grating: A holographic window to dynamic processes. *Accounts of chemical research*, 25(5):227–233, 1992.
- [15] Jeremy A Johnson, AA Maznev, John Cuffe, Jeffrey K Eliason, Austin J Minnich, Timothy Kehoe, Clivia M Sotomayor Torres, Gang Chen, and Keith A Nelson. Direct measurement of room-temperature nondiffusive thermal transport over micron distances in a silicon membrane. *Physical review letters*, 110(2):025901, 2013.
- [16] F Bencivenga, R Cucini, Flavio Capotondi, A Battistoni, R Mincigrucchi, E Giangrisostomi, A Gessini, M Manfredda, IP Nikolov, E Pedersoli, et al. Four-wave mixing experiments with extreme ultraviolet transient gratings. *Nature*, 520(7546):205–208, 2015.
- [17] Filippo Bencivenga, R Mincigrucchi, F Capotondi, L Foglia, D Naumenko, AA Maznev, E Pedersoli, A Simoncig, F Caporaletti, Vazrik Chiloyan, et al. Nanoscale transient gratings excited and probed by extreme ultraviolet femtosecond pulses. *Science advances*, 5(7):eaaw5805, 2019.
- [18] AA Maznev, F Bencivenga, Andrea Cannizzo, F Capotondi, R Cucini, RA Duncan, Thomas Feuerer, TD Frazer, L Foglia, H-M Frey, et al. Generation of coherent phonons by coherent extreme ultraviolet radiation in a transient grating experiment. *Applied physics letters*, 113(22), 2018.

- [19] Jeremy R Rouxel, Danny Fainozzi, Roman Mankowsky, Benedikt Rösner, Gediminas Seniutinas, Riccardo Mincigrucci, Sara Catalini, Laura Foglia, Riccardo Cucini, Florian Döring, et al. Hard x-ray transient grating spectroscopy on bismuth germanate. *Nature Photonics*, 15(7):499–503, 2021.
- [20] John T Fourkas, Rick Trebino, and MD Fayer. The grating decomposition method: A new approach for understanding polarization-selective transient grating experiments. i. theory. *The Journal of chemical physics*, 97(1):69–77, 1992.
- [21] John T Fourkas, Rick Trebino, and MD Fayer. The grating decomposition method: A new approach for understanding polarization-selective transient grating experiments. ii. applications. *The Journal of chemical physics*, 97(1):78–85, 1992.
- [22] Masahide Terazima. A new method for circular dichroism detection using cross-polarized transient grating. *The Journal of Physical Chemistry*, 99(7):1834–1836, 1995.
- [23] Masahide Terazima. A transient grating detection method of circular dichroism. *Molecular Physics*, 88(5):1223–1236, 1996.
- [24] Eléonore Roussel, Enrico Allaria, Carlo Callegari, Marcello Coreno, Riccardo Cucini, Simone Di Mitri, Bruno Diviacco, Eugenio Ferrari, Paola Finetti, David Gauthier, et al. Polarization characterization of soft x-ray radiation at fermi fel-2. In *Photonics*, volume 4, page 29. MDPI, 2017.
- [25] Enrico Allaria, Bruno Diviacco, Carlo Callegari, Paola Finetti, Benoît Mahieu, Jens Viefhaus, Marco Zangrando, Giovanni De Ninno, Guillaume Lambert, Eugenio Ferrari, et al. Control of the polarization of a vacuum-ultraviolet, high-gain, free-electron laser. *Physical Review X*, 4(4):041040, 2014.
- [26] Shaul Mukamel. *Principles of nonlinear optical spectroscopy*. Oxford University Press, 1995.
- [27] David Parker Craig and Thiru Thirunamachandran. *Molecular quantum electrodynamics: an introduction to radiation-molecule interactions*. Courier Corporation, 1998.
- [28] Thomas Rappen, Ulf-Gereon Peter, Martin Wegener, and Wilfried Schäfer. Polarization dependence of dephasing processes: A probe for many-body effects. *Physical Review B*, 49(15):10774, 1994.
- [29] Ingolf Warnke and Filipp Furche. Circular dichroism: electronic. *Wiley Interdisciplinary Reviews: Computational Molecular Science*, 2(1):150–166, 2012.
- [30] Hans-Joachim Werner, Peter J Knowles, Frederick R Manby, Joshua A Black, Klaus Doll, Andreas Heßelmann, Daniel Kats, Andreas Köhn, Tatiana Korona, David A Kreplin, et al. The molpro quantum chemistry package. *The Journal of chemical physics*, 152(14), 2020.
- [31] Christophe Nicolas and Catalin Miron. Lifetime broadening of core-excited and-ionized states. *Journal of Electron Spectroscopy and Related Phenomena*, 185(8-9):267–272, 2012.
- [32] AS Morillo-Candas, A Al-Haddad, S Augustin, A Cannizzo, Y Deng, T Feurer, J Knurr, C Ott, E Prat, M Rebholz, et al. All x-ray four-wave mixing on a gas phase sample. In *The European Conference on Lasers and Electro-Optics*, page jsi.1.2. Optica Publishing Group, 2023.